RSC Advances

COMMUNICATION

Cite this: *RSC Adv.*, 2016, **6**, 90489

Received 1st August 2016
Accepted 14th September 2016

DOI: 10.1039/c6ra19425g

www.rsc.org/advances

General fabrication of mesoporous Nb_2O_5 nanobelts for lithium ion battery anodes†

Chao Huang,[a] Jijiang Fu,[a] Hao Song,[a] Xiaofang Li,[a] Xiang Peng,[b] Biao Gao,*[a] Xuming Zhang*[a] and Paul K. Chu[b]

Mesoporous Nb_2O_5 nanobelts (NBs) have been synthesized by sequential thermal treatment of solid Nb_2O_5 NBs in NH_3 and air, which exhibit better crystallinity and a larger specific area (29.76 $m^2\ g^{-1}$) than that of solid Nb_2O_5 NBs (8.86 $m^2\ g^{-1}$) and exhibit a high capacity and good rate capability.

Introduction

In order to obtain high energy and power densities, good rate capability, and long cycling life, a desirable approach is to reduce the diffusion length of Li ions in lithium-ion batteries (LIBs) during the charging/discharging process and increase the interfacial contact area between the active materials and the electrolyte.[1,2] In this respect, a porous microstructure favors the improvement of the electrochemical behavior of active materials due to the easy penetration of ions and accommodation of volume expansion during lithiation/delithiation.[3] Yu *et al.* have produced a porous MoO_3 film by low-temperature thermal oxidation of nanostructured MoS_2 in air and the materials showed very good rate performance and high capacity as a result of the improved Li^+ diffusion kinetics in the small grains and widespread nanoholes.[4] Liu *et al.* have prepared two-dimensional (2D) mesoporous WO_{3-x}/graphene with a high reversible capacity of 748 mA h g^{-1} at 0.1C as well as good rate capability and stability because the porous structure facilitated electron and Li^+ diffusion.[5] These reports indicate that the mesoporous structure is a useful architecture to elevate the electrochemical performance of active materials in LIBs.

Recently, among those transition metal oxides (TMOs), orthorhombic niobium pentoxide (T-Nb_2O_5) has attracted much interest in lithium storage because of its high theoretical capacity, non-toxicity, robust corrosion resistance, as well as rapid ionic transport between the (001) planes.[6–8] Various fabrication approaches have been attempted to fabricate the mesoporous Nb_2O_5. Li *et al.* have prepared the mesoporous Nb_2O_5 with nonuniform macropores around 200 nm by template methods followed by annealing in air.[9] Wang *et al.* have synthesized mesoporous Nb_2O_5 nanosheets with the pore size in the range from 3 to 20 nm by vapor hydrolysis method at 600 °C in the presence of template of graphene–silica nanosheet.[10] Kong *et al.* have fabricated mesoporous Nb_2O_5@carbon core–shell structure with pore diameter of 2–3 nm using three steps oxidation.[11] Chen *et al.* have shown the mesoporous Nb_2O_5 with the pore size between 4.3 and 7.5 nm *via* complex template method.[12] Obviously, these techniques used to prepare mesoporous structure always suffer from long time preparation, complex process and specific template. Thus, a challenging work is remained to seek a simple and efficient technique for the preparation of porous TMOs.

Herein, a sequential thermal treatment of solid T-Nb_2O_5 NBs in NH_3 and air is described to fabricate porous T-Nb_2O_5 NBs. *Via* nitridation of solid T-Nb_2O_5 NBs, the structure contraction from orthorhombic cell (T-Nb_2O_5) to tetragonal cell (Nb_4N_5) is occurred by etching of NH_3,[21,22] which induces the formation of porous structure because of the volumetric shrinking. After following oxidization in air, the mesoporous T-Nb_2O_5 NBs with a larger specific surface area was prepared, as illustrated in Fig. 1a. The reserved pores are evenly distributed on the T-Nb_2O_5 NBs and can be easily modulated by controlling temperature.[13–16] More importantly, the simple, low risk, and controllable method is in favor of the high crystallinity than other methods, such as anodization and vapor-phase hydrolysis,[10,17] because of the elevation of oxidation efficiency in both inner and outer surface of mesoporous structure, resulting in good electrochemical performances.[18] Consequently, a reversible capacity of about 400 mA h g^{-1} is achieved at 0.05 A g^{-1}, which is much close to its theoretical capacity and higher than that of the solid Nb_2O_5 NBs (350 mA h g^{-1} at 0.05 A g^{-1}). The results demonstrate a simple and effective approach to fabricate

[a]*The State Key Laboratory of Refractories and Metallurgy, Wuhan University of Science and Technology, Wuhan 430081, China. E-mail: xumzhang@wust.edu.cn; gaobiao@wust.edu.cn*

[b]*Department of Materials Science and Physics, City University of Hong Kong, Tat Chee Avenue, Kowloon, Hong Kong, China*

† Electronic supplementary information (ESI) available. See DOI: 10.1039/c6ra19425g

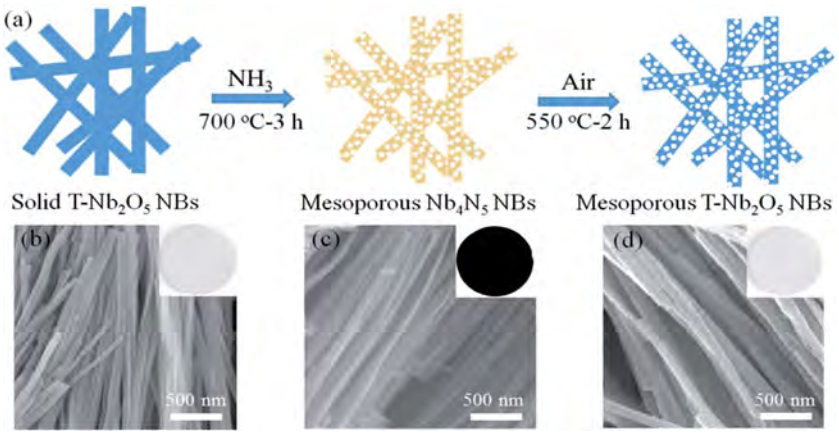

Fig. 1 (a) Schematic illustration of the preparation procedures. (b)–(d) SEM images; the insets are the corresponding digital pictures.

mesoporous T-Nb_2O_5 NBs for anode materials with enhanced electrochemical performance in LIBs and it can be readily extended to the production of different types of mesoporous TMOs.

Experimental methods

Synthesis of mesoporous Nb_2O_5 nanobelts

All the chemicals were purchased from Sigma and used without purification. The solid Nb_2O_5 NBs were synthesized by hydrothermal treatment, ion exchange and annealing in air. In brief, 0.26 g of niobium (Nb) powders (99.5%) were dissolved in 40 mL of 10 M NaOH under stirring for 10 min and transferred to a 60 mL Teflon-lined stainless steel autoclave. After heating at 130 °C for 18 h in an oven, the products were filtered and rinsed with deionized water several times to obtain the sodium niobate NBs. The niobic acid NBs were obtained after ion exchange in diluted HCl and more details about the synthesis can be found from our previous paper.[13] The protonated products were rinsed with deionized water to obtain a neutral pH and then dried at 80 °C overnight. Then, the solid Nb_2O_5 NBs was achieved after annealing at 700 °C for 3 h in air. To prepare the mesoporous Nb_2O_5 NBs, the solid T-Nb_2O_5 NBs were thermally treated in ammonia (NH_3) ambient at 700 °C for 3 h and then in air at 550 °C for 2 h. Finally, the products were collected after cooling to room temperature.

Materials characterization

The morphology, structure, and composition of the samples were determined by field-emission scanning electron microscopy (FE-SEM, FEI nanoSEM 450), transmission electron microscopy (TEM, FEI Titan 60-300 Cs), X-ray diffraction using the Cu Kα radiation (λ = 1.5418 Å) (XRD, Philips X' Pert Pro), and X-ray photoelectron spectroscopy (XPS, ESCALB MK-II). The surface area and pore size distribution were determined by N_2 adsorption (Micromeritics, ASAP 2020 analyzer) and the specific surface area was calculated from the N_2 adsorption isotherm based on the BET equation.

Electrochemical measurements

The coin-type half-cells was assembled based on the solid T-Nb_2O_5 NBs and mesoporous T-Nb_2O_5 NBs in an argon-filled glove-box (Vigor SG1200/750TS-C). A polypropylene membrane (Celgard 2400) was used as the separator and a lithium foil served as the counter and reference electrodes. 1 M $LiPF_6$ in ethylene carbonate (EC)/dimethylcarbonate (DME) (1 : 1 by volume) as the electrolyte. Galvanostatic charge–discharge (GCD) tests were conducted on a LAND battery program-control system (Wuhan, Land CT2001A) in the voltage range between 0.01 and 3.0 V (*vs.* Li/Li^+) at different current densities and cyclic voltammetry (CV) was conducted on an electrochemical analyzer (CHI 760e) between 0.01 and 3.0 V (*vs.* Li/Li^+) at a scanning rate of 0.2 mV s^{-1}. Electrochemical impedance spectroscopy (EIS) was carried out in the frequency range between 0.1 Hz and 100 kHz at the open-circuit potential with an alternating current (AC) perturbation of 5 mV.

Results and discussion

Fig. 1a illustrates the preparation procedures of the mesoporous T-Nb_2O_5 NBs. The solid Nb_2O_5 NBs were annealed in NH_3 and then oxidized in air. Fig. 1b–d show the morphological evolution revealing that the solid NBs have a diameter of about 100 nm and are dozens of micrometers long (Fig. S1†). After nitridation, the mesoporous structure is produced (Fig. 1c) and preserved after subsequent oxidization in air. The color of the materials changes from white to black during nitridation but back to white again after oxidation.

The XRD patterns of the materials are presented in Fig. 2a. The crystalline phase of the solid Nb_2O_5 NBs can be indexed to the orthorhombic cell of Nb_2O_5 (T-Nb_2O_5, JCPDS no. 30-0873),[8,19] whereas the characteristic peaks of the nitrided product at 35.9°, 42°, and 60.5° can be indexed to tetragonal Nb_4N_5 (JCPDS no. 51-1327).[20] After oxidation, the mesoporous T-Nb_2O_5 NBs have the same crystalline phase as the solid T-Nb_2O_5 NBs in addition to new (130) and (060) planes suggesting better crystallization. The full-scan XPS of the solid and mesoporous T-Nb_2O_5 NBs have high purity because no other peaks appear

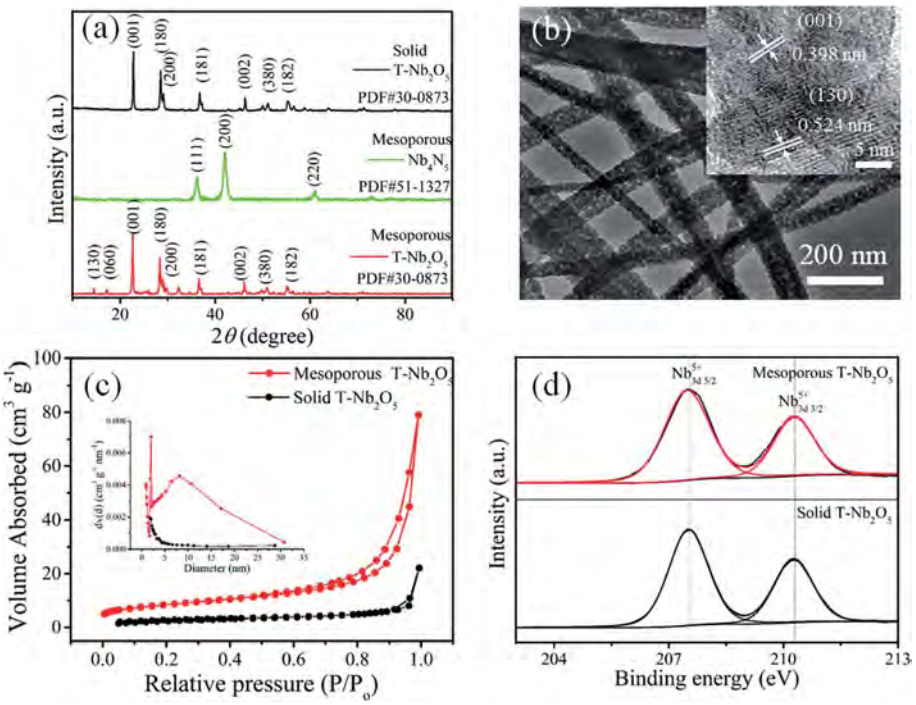

Fig. 2 (a) XRD patterns; (b) TEM and HRTEM (insert) images of mesoporous T-Nb_2O_5; (c) N_2 adsorption–desorption isotherm (inset picture showing the BJH desorption pore size distribution); (d) fine XPS spectra of Nb 3d of solid and mesoporous T-Nb_2O_5.

except Nb, C, O, N (Fig. S2†). The low- and high-resolution TEM images in Fig. 2b disclose that the NBs (50–100 nm width) are porous structure and the pores about 10 nm distribute evenly on NBs whereas the solid T-Nb_2O_5 NBs have uniform structure (Fig. S3†). The HRTEM image in the insert of Fig. 2b reveals a crystalline structure with the representative lattice plane distances of 0.398 and 0.524 nm which match well with the *d*-spacing of (001) and (130) planes of orthorhombic Nb_2O_5, respectively.[21] The Brunauer–Emmett–Teller (BET) analysis shown in Fig. 2c indicates that the surface area of the mesoporous T-Nb_2O_5 NBs is as large as 29.76 $m^2\ g^{-1}$ which is about 3 times larger than that of the solid T-Nb_2O_5 NBs (8.86 $m^2\ g^{-1}$). The distributions of pores size in mesoporous structure fasten on 2 nm and 10 nm. In this preparation process, the solid Nb_2O_5 NBs were firstly converted to the corresponding mesoporous metal nitrides by nitridation in NH_3 according to the previous reports.[22,23] Due to the structure changing from orthorhombic Nb_2O_5 (cell volume about 810 $Å^3$) to tetragonal Nb_4N_5 (cell volume about 205 $Å^3$),[24,25] large numbers of mesopores can be produced due to the volumetric shrinking.[12] Subsequently, the mesoporous T-Nb_2O_5 NBs were obtained again when the mesoporous Nb_4N_5 NBs were re-oxidized in air. However, the decreasing specific area from mesoporous Nb_4N_5 to mesoporous T-Nb_2O_5 NBs is observed as a result of the volume expansion of mesopores structure after re-oxidation (Fig. S4†). It can be seen that the specific surface area of re-oxidized T-Nb_2O_5 (29.76 $m^2\ g^{-1}$) is smaller than that of mesoporous Nb_4N_5 NBs (38.6 $m^2\ g^{-1}$) as well as the decreased integrated pore volume from 116 $cm^3\ g^{-1}$ of mesoporous Nb_4N_5 NBs to 80 $cm^3\ g^{-1}$ of mesoporous T-Nb_2O_5 NBs, indicating the expansion of mesoporous structure after re-oxidation, as shown in Fig. 1b–d. Fig. 2d depicts the high-resolution Nb 3d XPS spectra, which can be fitted by two sub-peaks at 207.2 eV and 205.8 eV attributable to the spin–orbit doublet of Nb $3d_{3/2}$ and Nb $3d_{5/2}$ of Nb^{5+} in oxide, respectively.[26,27]

The electrochemical properties of the coin-type half-cells composed of the solid/mesoporous T-Nb_2O_5 NBs and Li metal foil serving as the active and counter electrodes, respectively, are determined by cyclic voltammetry (CV), galvanostatic charge discharge (GCD) and electrochemical impedance spectroscopy (EIS). Fig. 3a shows the CV profiles acquired in the potential range between 0 and 3 V (V *vs.* Li/Li^+) at a scanning rate of 0.2 mV s^{-1}. The cathodic peak at 1.6–1.4 V (*vs.* Li^+/Li) can be attributed to Li^+ intercalated into Nb_2O_5.[28] While the anodic peak located at 1.7–2.0 V (*vs.* Li^+/Li) should be attributed to Li^+ deintercalated from $Li_xNb_2O_5$. An irreversible chemical reaction occurs at 0.77 V during the first discharging process probably due to the formation of a solid electrolyte interface (SEI) layer.[29] The electrochemical Li ions insertion–deinsertion mechanism of Nb_2O_5 can be expressed as follow:[30,31]

$$xLi^+ + xe^- + Nb_2O_5 \leftrightarrow Li_xNb_2O_5 \quad (1)$$

In fact, the capacity of Nb_2O_5 in LIBs results from the reversible chemical reaction between Nb^{5+} and Nb^{3+} within the potential range from 0 to 3 V *vs.* Li^+/Li.[30,31] According to the reaction formula above, the theoretical capacity for the chemical reaction of Li ions intercalation/deintercalation in Nb_2O_5 is calculated to be 403 mA h g^{-1} (see ESI†). Fig. 3b shows the GCD profiles of mesoporous Nb_2O_5 NBs and solid Nb_2O_5 NBs for the first three cycles. It can be seen that the stable capacity of

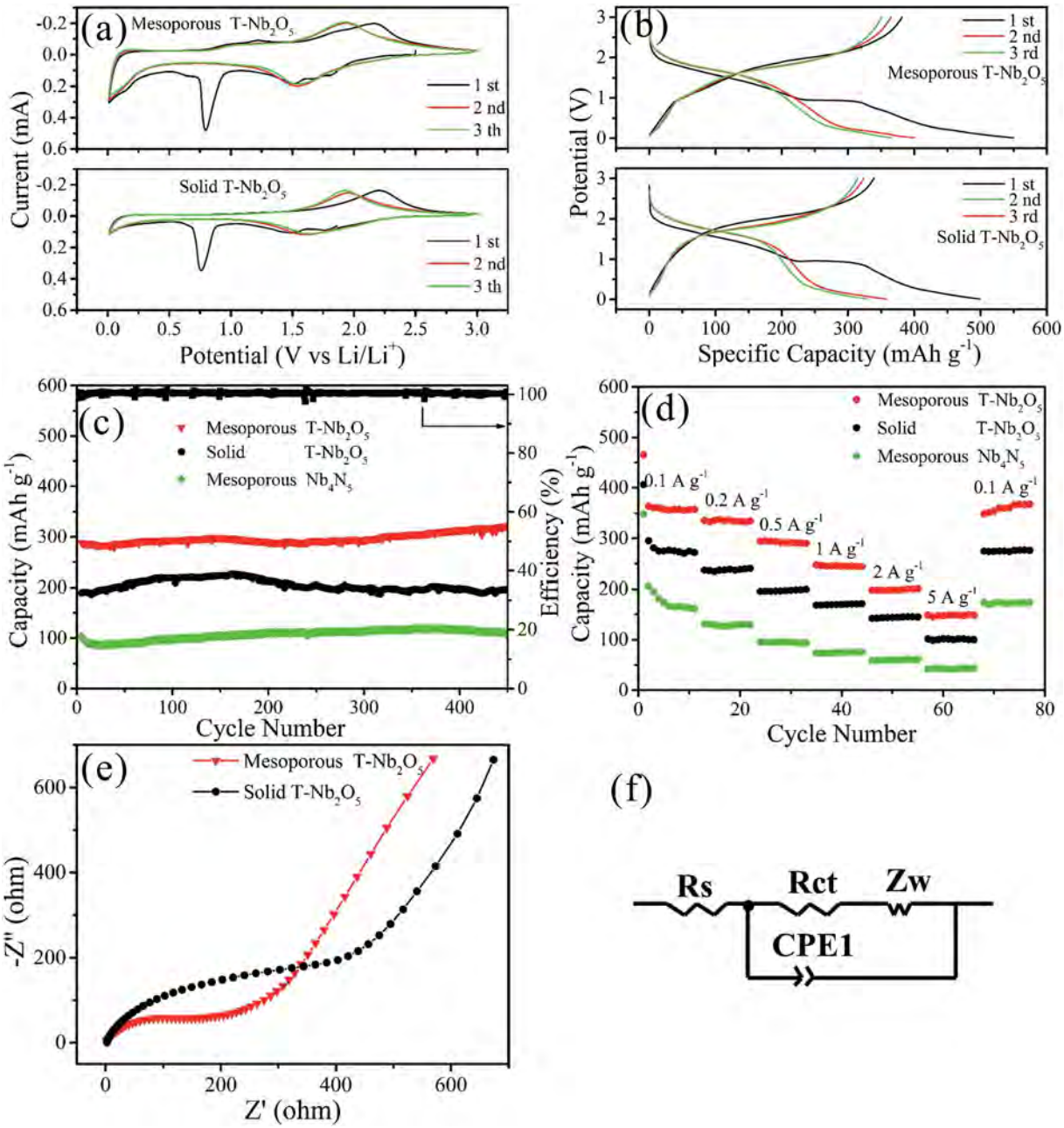

Fig. 3 (a) CV curves (at 0.2 mV s^{-1}); (b) GCD curves (at 0.05 A g^{-1}); (c) cycling performance (at 0.5 A g^{-1}); (d) rate capability; (e) EIS plots; (f) equivalent circuit models.

mesoporous Nb_2O_5 is about 400 mA h g^{-1} at a current density of 0.05 A g^{-1} which is much close to its theoretical capacity, and higher than that of the solid Nb_2O_5 NBs (~357 mA h g^{-1}). However, because of the high specific area and the formation of SEI film at first cycle, the initial coulombic efficiency for mesoporous Nb_2O_5 NBs (69.3%) is lower than that of solid Nb_2O_5 NBs (72.3%). Fig. 3c shows the cycling stability of the solid T-Nb_2O_5 NBs, mesoporous T-Nb_2O_5 NBs, and mesoporous Nb_4N_5 NBs for 450 cycles (at 0.5 A g^{-1} in 0.01–3.0 V). After first three GCD cycles at 0.05 A g^{-1}, the mesoporous T-Nb_2O_5 NBs deliver a capacity as high as 300 mA h g^{-1} with an reversible coulombic efficiency of about 100% when the current density increases to 0.5 A g^{-1} which is higher than that of the solid T-Nb_2O_5 NBs (192 mA h g^{-1}), mesoporous Nb_4N_5 NBs (109 mA h g^{-1}), and exhibits larger capacitance and better cycling stability than that of previously reported nanopowders Nb_2O_5 and unchin-like Nb_2O_5 microspheres.[29,32] The higher reversible capacity of mesoporous Nb_2O_5 is achieved due to the large surface area and short ions diffusion distance provided by mesoporous structure for high efficient Li^+ intercalation/deintercalation. Inversely, the mesoporous Nb_4N_5 NBs show poor capacity for LIBs as a result of few chemical valence changing of $Nb^{3.75+}$ for Nb_4N_5 (*vs.* Nb^{5+} for Nb_2O_5) to Nb^{3+} after the intercalation of Li ions.[30] The rate capability of the mesoporous T-Nb_2O_5 NBs, solid T-Nb_2O_5 NBs

and mesoporous Nb_4N_5 NBs are shown in Fig. 3d. A reversible average capacity decreased from 356 to 148 mA h g^{-1} (about 41.6% capacitance retention) is observed from mesoporous Nb_2O_5 when the current density is increased from 0.1 to 5 A g^{-1} and it recovered to over 362 mA h g^{-1} when the current density is returned to 0.1 A g^{-1}. In contrary, the solid T-Nb_2O_5 NBs and mesoporous Nb_4N_5 NBs show poorer reversible capacities of 276 mA h g^{-1} and 168 mA h g^{-1} at 0.1 A g^{-1} as well as 36.6% (101 mA h g^{-1}) and 25.6% (43 mA h g^{-1}) retention at 5 A g^{-1}. The superior rate capability of the mesoporous T-Nb_2O_5 NBs can be attributed to the better Li^+ diffusion kinetics which is revealed by EIS as shown in Fig. 3e. The charge transfer resistances of the solid and mesoporous T-Nb_2O_5 NBs derived from the intercept of the plot on the real axis are 408 and 210 Ω, respectively, indicating fast charge transfer in the mesoporous structure.

Conclusion

Mesoporous T-Nb_2O_5 NBs synthesized by sequential thermal treatment in NH_3 and air have a larger specific area of 29.76 m^2 g^{-1} and better crystallinity than the solid T-Nb_2O_5 NBs in addition to larger capacity, excellent rate capability and stable cycling performance. A reversible capacity of 356 mA h g^{-1} is achieved at 0.1 A g^{-1} and over 41.6% of the initial capacitance is retained when the current density is increased to 5 A g^{-1}. Therefore, the mesoporous T-Nb_2O_5 NBs are promising anode materials in LIBs and the simple strategy of fabrication can be extended to prepare other mesoporous TMOs.

Acknowledgements

This work was financially supported by Natural Science Foundation of China (51504171, 51572100, 31500783), Project of Hubei Provincial Education Office (B2015346), Young Science Foundation of The State Key Laboratory of Refractories and Metallurgy of Wuhan University of Science and Technology (2016QN08), Project of Natural Science Foundation of Hubei Province (2015CFA116), and City University of Hong Kong Applied Research Grant (ARG) No. 9667122.

References

1 S. Wang, Z. D. Lu, D. Wang, C. G. Li, C. H. Chen and Y. D. Yin, *J. Mater. Chem. A*, 2011, **21**, 6365–6369.
2 B. Philippe, M. Hahlin, K. Edström, T. Gustafsson, H. Siegbahn and H. Rensmo, *J. Electrochem. Soc.*, 2016, **163**, A178–A191.
3 G. Y. Zhao, N. Q. Zhang and K. N. Sun, *J. Mater. Chem. A*, 2013, **1**, 221–224.
4 X. Y. Yu, L. Wang, J. F. Liu and X. M. Sun, *ChemElectroChem*, 2014, **1**, 1476–1479.
5 F. Liu, J. G. Kim, C. W. Lee and J. S. Im, *Appl. Surf. Sci.*, 2014, **316**, 604–609.
6 V. Augustyn, J. Come, M. A. Lowe, J. W. Kim, P. L. Taberna, S. H. Tolbert, H. D. Abruña, P. Simon and B. Dunn, *Nat. Mater.*, 2013, **12**, 518–522.
7 M. D. Wei, K. M. Wei, M. Ichihara and H. S. Zhou, *Electrochem. Commun.*, 2008, **10**, 980–983.
8 X. L. Wang, G. Li, Z. Chen, V. Augustyn, X. M. Ma, G. Wang, B. Dunn and Y. F. Lu, *Adv. Energy Mater.*, 2011, **1**, 1089–1093.
9 S. Li, C. N. Schmidt, Q. Xu, X. Cao and G. Cao, *ChemNanoMat*, 2016, **2**, 675–680.
10 L. Wang, X. F. Bi and S. B. Yang, *Adv. Mater.*, 2016, **28**, 7672–7679.
11 L. P. Kong, C. F. Zhang, J. T. Wang, W. M. Qiao, L. C. Ling and D. H. Long, *Sci. Rep.*, 2016, **6**, 21177.
12 X. Y. Chen, T. Yu, X. X. Fan, H. T. Zhang, Z. S. Li, J. H. Ye and Z. L. Zou, *Appl. Surf. Sci.*, 2007, **253**, 8500–8506.
13 B. Gao, X. Xiao, J. J. Su, X. M. Zhang, X. Peng, J. J. Fu and P. K. Chu, *Appl. Surf. Sci.*, 2016, **383**, 57–63.
14 X. Peng, W. Li, L. Wang, L. S. Hu, W. H. Jin, A. Gao, X. M. Zhang, K. F. Huo and P. K. Chu, *Electrochim. Acta*, 2016, **214**, 201–207.
15 D. Choi, G. E. Blomgren and P. N. Kumta, *Adv. Mater.*, 2006, **18**, 1178–1182.
16 D. W. Choi and P. N. Kumta, *Electrochem. Solid-State Lett.*, 2005, **8**, A418–A422.
17 K. Kim, M. S. Kim, P. R. Cha, S. H. Kang and J. H. Kim, *Chem. Mater.*, 2016, **28**, 1453–1461.
18 K. Brezesinski, J. Wang, J. Haetge, C. Reitz, S. O. Steinmueller, S. H. Tolbert, B. M. Smarsly, B. Dunn and T. Brezesinski, *J. Am. Chem. Soc.*, 2010, **132**, 6982–6990.
19 R. Kodama, Y. Terada, I. Nakai, S. Komaba and N. Kumagai, *J. Electrochem. Soc.*, 2006, **153**, A583–A588.
20 H. Cui, G. Zhu, X. Liu, F. Liu, Y. Xie, C. Yang, T. Lin, H. Gu and F. Huang, *Adv. Sci.*, 2015, **2**, 1500126.
21 G. Q. Ma, K. Li, Y. Y. Li, B. Gao, T. P. Ding, Q. Zhong, J. Su, L. Gong, J. Chen, L. y. Yuan, B. Hu, J. Zhou and K. F. Huo, *ChemElectroChem*, 2016, **3**, 1360–1368.
22 P. Y. Wang, R. T. Wang, J. W. Lang, X. Zhang, Z. K. Chen and X. B. Yan, *J. Mater. Chem. A*, 2016, **4**, 9760–9766.
23 X. Xiao, X. Peng, H. Y. Jin, T. Q. Li, C. C. Zhang, B. Gao, B. Hu, K. F. Huo and J. Zhou, *Adv. Mater.*, 2013, **25**, 5091–5097.
24 K. Kato and S. Tamura, *Acta Crystallogr., Sect. B: Struct. Crystallogr. Cryst. Chem.*, 1975, **31**, 673–677.
25 N. Terao, *J. Less-Common Met.*, 1971, **23**, 159–169.
26 S. Li, Q. Xu, E. Uchaker, X. Cao and G. Z. Cao, *CrystEngComm*, 2016, **18**, 2532–2540.
27 W. B. Zhang, W. D. Wu, X. M. Wang, X. L. Cheng, D. W. Yan, C. L. Shen, L. P. Peng, Y. Y. Wang and L. Bai, *Surf. Interface Anal.*, 2013, **45**, 1206–1210.
28 A. Viet, M. Reddy, R. Jose, B. Chowdari and S. Ramakrishna, *J. Phys. Chem. C*, 2009, **114**, 664–671.
29 H. Lu, K. Xiang, N. Bai, W. Zhou, S. Wang and H. Chen, *Mater. Lett.*, 2016, **167**, 106–108.
30 X. Wang, C. Yan, J. Yan, A. Sumboja and P. S. Lee, *Nano Energy*, 2015, **11**, 765–772.
31 H. Y. Lu, K. X. Xiang, N. B. Bai, W. Zhou, S. L. Wang and H. Chen, *Mater. Lett.*, 2016, **167**, 106–108.
32 M. Lübke, A. Sumboja, I. D. Johnson, D. J. L. Brett, P. R. Shearing, Z. Liu and J. A. Darr, *Electrochim. Acta*, 2016, **192**, 363–369.